Fully Fused Quinoidal/Aromatic Carbazole Macrocycles with Poly-radical Characters

Soumyajit Das,[†] Tun Seng Herng,[‡] José L. Zafra,[§] Paula Mayorga Burrezo,[§] Masaaki Kitano,[∥] Masatoshi Ishida,[⊥] Tullimilli Y. Gopalakrishna,[†] Pan Hu,[†] Atsuhiro Osuka,[∥] Juan Casado,[*,§] Jun Ding,[*,‡] David Casanova,[*,#] and Jishan Wu[*,†]

[†]Department of Chemistry, National University of Singapore, 3 Science Drive 3, 117543 Singapore

[‡]Department of Materials Science & Engineering, National University of Singapore, 119260 Singapore

[§]Department of Physical Chemistry, University of Malaga, Campus de Teatinos s/n, 29071 Malaga, Spain

[∥]Department of Chemistry, Graduate School of Science, Kyoto University, Sakyo-ku, Kyoto 606-8502, Japan

[⊥]Department of Chemistry and Biochemistry, Graduate School of Engineering and Center for Molecular Systems, Kyushu University, 744 Motooka, Nishi-ku, Fukuoka 819-0395, Japan

[#]IKERBASQUE - Basque Foundation for Science & Donostia International Physics Center & Kimika Fakultatea, Euskal Herriko Unibertsitatea, Paseo Manuel de Lardizabal, 4, 20018 Donostia-San Sebastián, Euskadi, Spain

S *Supporting Information*

ABSTRACT: While the chemistry of open-shell singlet diradicaloids has been successfully developed in recent years, the synthesis of π-conjugated systems with poly-radical characters (i.e., beyond diradical) in the singlet ground state has been mostly unsuccessful. In this study, we report the synthesis and isolation of two fully fused macrocycles containing four (**4MC**) and six (**6MC**) alternatingly arranged quinoidal/aromatic carbazole units. Ab initio electronic structure calculations and various experimental measurements indicate that both **4MC** and **6MC** have an open-shell singlet ground state with moderate tetraradical and hexaradical characters, respectively. Both compounds can be thermally populated to high-spin excited states, resulting in weak magnetization at room temperature. Our study represents the first demonstration of singlet π-conjugated molecules with poly-radical characters and also gives some insights into molecular magnetism in neutral π-conjugated polycyclic heteroarenes.
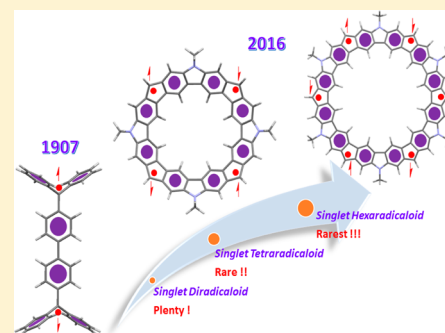
INTRODUCTION

π-Conjugated molecules with open-shell singlet ground states[1] have drawn immense attention from researchers worldwide due to their unique optical, electronic, and magnetic properties that make them attractive for nonlinear optical materials,[2] field effect transistors,[3] and organic spintronics.[4] Successful isolation of various relatively stable diradicaloids[5−10] motivates us to work toward molecules with poly-radical characters. Theoretically, graphene nanoribbons (including long acenes) with elongated zigzag edges may develop diradical and even poly-radical characters in the electronic ground state.[11] This behavior has been experimentally validated in small-size polycyclic aromatic hydrocarbons (PAHs) such as teranthene and quarteranthene, which show moderate to large diradical characters.[9] However, synthesis and isolation of PAHs beyond diradicals, i.e., with higher radical characters in the singlet ground state, remains a challenging task due to tedious synthesis and their intrinsic instability. Recently, Tobe et al. reported a hydrocarbon with potential tetraradical characters, the cyclic tetracyclopenta[*def,jkl,pqr,vwx*]tetraphenylene (TCPTP).[12] However, a sharp NMR spectrum at room

temperature combined with other experimental evidence implies that TCPTP behaves more like a closed-shell compound and can be better described as a singlet diradicaloid with moderate diradical characters and small tetraradical characters. Meanwhile, some of us synthesized a series of linear tetraradicaloids based on fused heptazethrene dimer (HZD) and its analogues, and again, all the experimental and theoretical studies revealed that they show very small tetraradical characters.[13] Therefore, singlet π-conjugated molecules with significant poly-radical characters still remain unknown. The difficulty in modeling organic molecules possessing poly-radical characters can be mainly ascribed to the strong anti-ferromagnetic bonding interactions between the multiple spins in the singlet ground state. In other words, the presence of strong poly-radicaloid nature in singlet ground-state molecules requires sufficient driving force from closed-shell form to open-shell diradical form and then to higher poly-radical forms. Previous studies have demonstrated that recovery
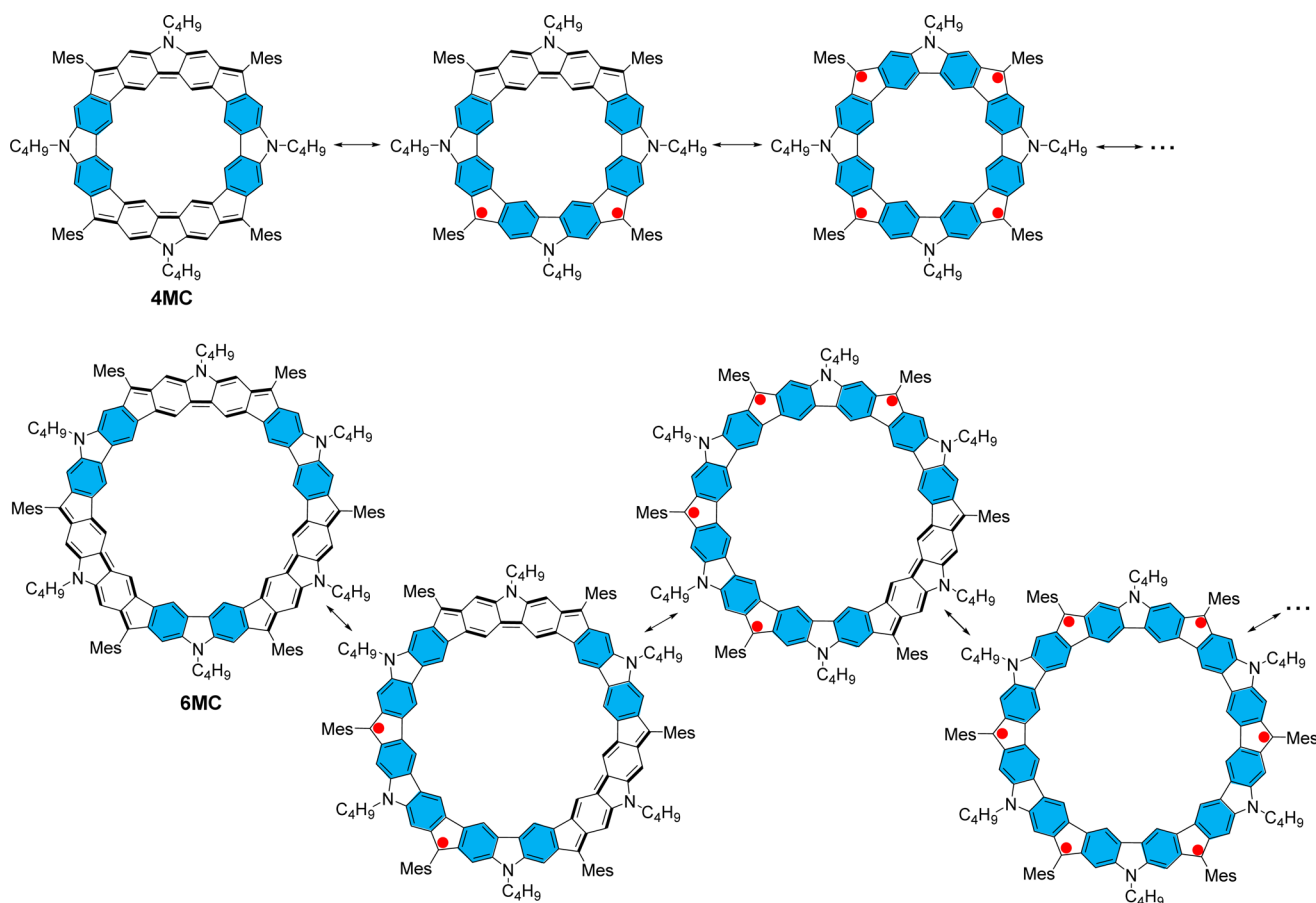
Figure 1. Closed-shell and open-shell canonical forms of **4MC** and **6MC**. Mes = mesityl groups. Clar's aromatic sextets are highlighted in blue hexagons.

of one or more aromatic sextet rings in the diradical form was one of the major driving forces to obtain molecules with a significant diradical character.[7c,9a] In TCTP and HZD, only one aromatic sextet ring is gained from closed-shell form to diradical form and then to tetraradical form, and this radical stabilization force may not be sufficient to extensively drive the molecules toward open-shell tetraradicaloids and turn out into very small tetraradical character. Therefore, we envision that increasing the driving force between each resonance form would be a feasible approach to attain larger poly-radical characters in these systems.

In this article, we report the design, challenging synthesis, and physical characterization of two fully fused carbazole macrocycles, **4MC** and **6MC**, which contain four and six alternatingly arranged quinoidal and aromatic carbazole units, respectively (Figure 1). The quinoidal carbazole moiety is fundamentally an analogue of pro-aromatic Tschitschibabin's hydrocarbon[14] and has an irresistible tendency to recover two aromatic sextet rings in the diradical form. Such a simple analysis can be applied to **4MC** and **6MC**, in which two aromatic sextets are gained at each stage of transition from closed-shell form to open-shell diradical form, and then to tetraradical form and finally to hexaradical form (Figure 1). Therefore, we predict larger driving force toward poly-radical ground state for both **4MC** and **6MC** compared to that of TCPTP and HZD cases. Bulky mesityl groups were attached to the cyclopenta rings to kinetically block the reactive sites as well as ensuring sufficient solubility. Various experimental measurements and advanced theoretical calculations indicate that both

compounds display desirable poly-radical characters in the singlet ground state. In addition, small energy differences to low-lying excited states are calculated and measured, which allow the molecules to easily populate to high-spin states that result in room-temperature magnetic activity.

RESULTS AND DISCUSSION

Synthesis and Structural Characterizations. The key intermediates for the synthesis of **4MC** and **6MC** are the tetra-aldehyde **4MC-CHO** and hexa-aldehyde **6MC-CHO**, which were synthesized by Suzuki coupling reaction between pre-synthesized **1**[15] and **2**[16] in the presence of $Pd_2(dba)_3$-[(t-Bu)$_3$PH]BF$_4$ catalyst, and isolated by recycling gel permeation chromatography in 2% and 29% yield, respectively (Scheme 1). The macrocyclic structures of **4MC-CHO** and **6MC-CHO** were unambiguously confirmed by single-crystal X-ray crystallographic analysis (Figure 2) along with ^{1}H and ^{13}C NMR and high-resolution atmospheric pressure chemical ionization mass spectral (HR APCI MS) analysis (see data in the Supporting Information (SI)). Dry tetrahydrofuran solutions of compounds **4MC-CHO** and **6MC-CHO** were then individually treated with 2-mesitylmagnesium bromide at room temperature to afford the respective tetracarbinol and hexacarbinol derivatives as racemic mixtures which, without further purifications, were dissolved in dichloromethane (DCM) and treated with BF$_3$·Et$_2$O to provide the ring-cyclized products **4MC-4H** and **6MC-6H** in 25% and 41% yield, respectively, as a mixture of diastereomers. The HR APCI MS and 2D NOESY
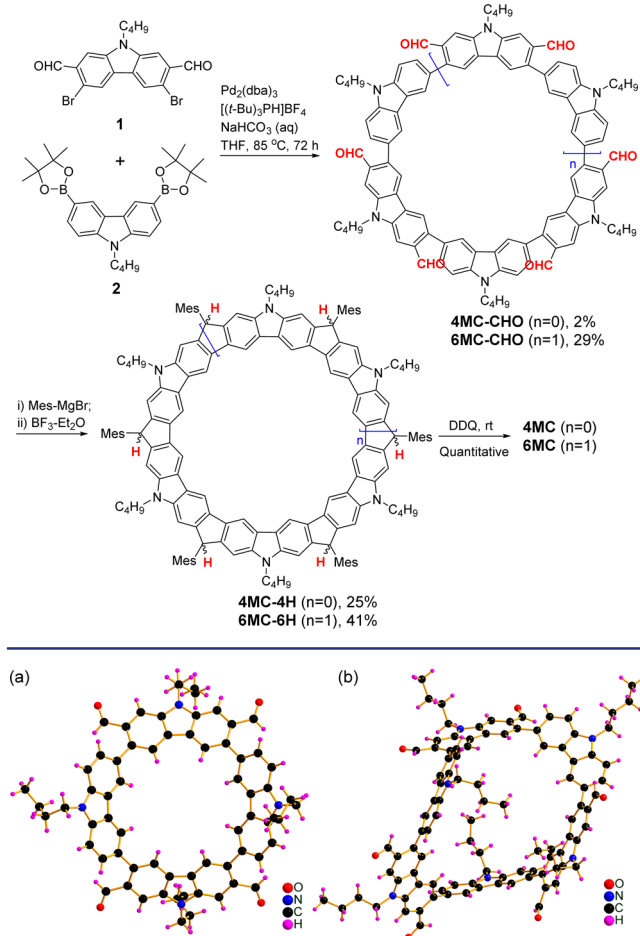
Scheme 1. Synthetic Route for 4MC and 6MC

4MC-CHO (n=0), 2%
6MC-CHO (n=1), 29%

4MC (n=0)
6MC (n=1)

4MC-4H (n=0), 25%
6MC-6H (n=1), 41%

Figure 2. X-ray crystallographic analysis of the macrocyclic precursors (a) **4MC-CHO** and (b) **6MC-CHO**.

NMR analysis support the formation of **4MC-4H** and **6MC-6H** (see detailed analysis in SI).

The final dehydrogenation step, monitored through MALDI-TOF MS (Figure S6 in SI), conducted by treating DCM solution of **4MC-4H** with portion wise addition of 4.2 equiv of 2,3-dichloro-5,6-dicyano-p-benzoquinone (DDQ), produced **4MC** in nearly quantitative yield. However, only 3 equiv of DDQ was necessary to fully convert **6MC-6H** to **6MC**. After completion of the reaction, careful evaporation of DCM solution at −20 °C was done. Compounds **4MC** and **6MC** are found to be unstable on silica gel or alumina column (even at −78 °C), but they can be purified by cross-linked polystyrene (bio-beads)-based size-exclusion chromatography. The small molecular weight DDQ and its reduced products stay at the baseline, leaving a clear band for the final product coming first. The MALDI-TOF mass spectra of the final products revealed the desired peaks with precise isotopic distribution patterns for **4MC** and **6MC** that were in perfect agreement with the simulated spectra (Figure 3). The HRMS analysis for both **4MC** and **6MC** further established their formation and are within the acceptable error range; however, the parent ion peak for the bigger macrocycle **6MC** appears at an m/z ($z = 2$) value of 1050.5742 (calcd 1050.5721) (Figures S7 and S8 in SI).

The ^1H NMR measurement of compound **4MC** revealed some weak-to-broad signals at the room temperature, and as the temperature was lowered to 0 °C, new signals (b,b′)
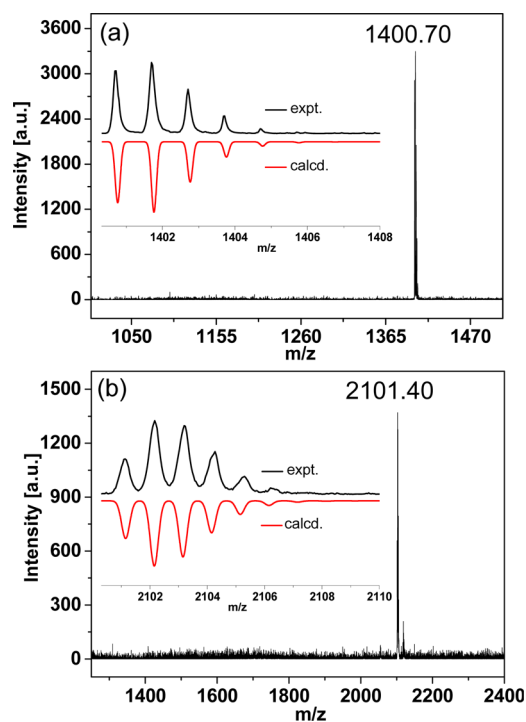

Figure 3. MALDI-TOF mass spectra of (a) **4MC** and (b) **6MC**. Inset is a comparison between the calculated and experimental isotopic distributions.

emerged which became sharper at −30 °C (Figure 4a, see proton labeling in Figure 4b). However, signals started to broaden again at −60 °C, likely due to the reduced solubility caused by aggregation at very low temperature. This observation is typical for many open-shell singlet diradicaolids, suggesting an open-shell singlet ground state for **4MC**.[7,9] The NMR signal broadening at 298 K can be attributed to a significant population of paramagnetic triplet species at room temperature; upon lowering the temperature, the equilibrium shifts to singlet species, affecting the NMR peaks (sharper and distinct). In the simulated gas-phase NMR spectrum of **4MC** in C_{2v} symmetry (UB3LYP/6-31G* computational level with mesityl and n-butyl groups replaced by hydrogen and methyl groups, respectively), the inner protons of the macrocycle ring (b, b′) appear at lower field 9.01 ppm while the outer protons (a, a′) at a higher field 4.71 ppm (Figure 4c). Accordingly, the experimental NMR signals at 10.62 ppm (2 integration) and −3.2 ppm (2 integration), belonging to overall 16 protons (4 × 2 inner H's and 4 × 2 outer H's), were assigned to inner and outer protons of the macrocycle core (see full spectrum and integration in Figure S16). This behavior is due to the moderate global anti-aromatic paratropic ring current effect that shifts downfield and upfield the signal of inner and outer ring protons, respectively. Nucleus independent chemical shift (NICS) calculations (at UB3LYP/6-31G* level of theory) show that the benzenoid rings in the carbazole macrocycle become non-aromatic (NICS(0) ≈ 0 ppm), and the z-axis NICS scan at the center of the macrocycle indicates a weak anti-aromatic character (small positive NICS values) of the whole system (Figure 4c). Indeed, anisotropy of the induced current density (AICD) plot of **4MC** clearly shows an anti-clockwise ring current delocalized along the periphery (escaping nitrogens) containing 36 (4n, n = 9) π electrons (Figure 4d). The N-containing five-membered rings are
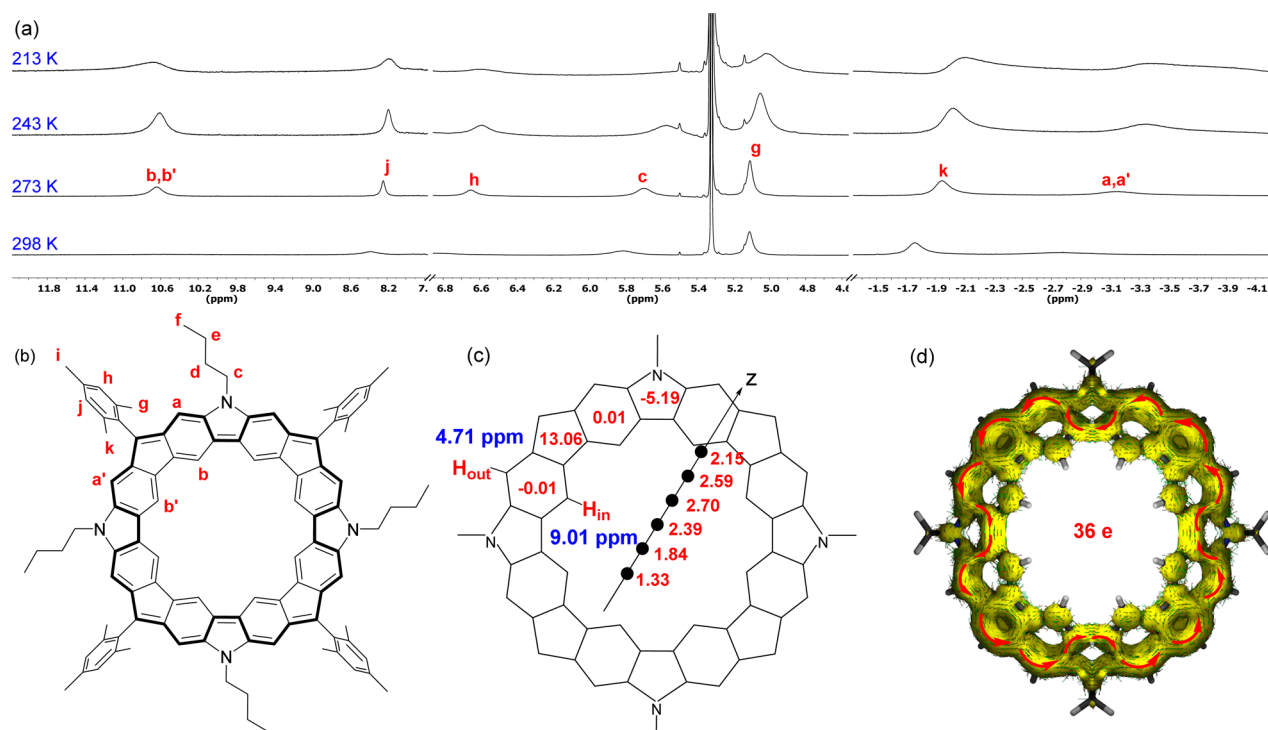
Figure 4. (a) Variable-temperature ^1H NMR spectra of **4MC** in CD_2Cl_2. (b) Labeling of **4MC** protons. (c) Calculated NICS(0) values and checmial shifts for **4MC** in C_{2v} symmetry, and a NICS scan along the z axis at the molecular center. (d) Calculated AICD plot of **4MC**; the red arrows indicate anti-clockwise ring current with a 36 π-electron conjugation pathway (also highlighted in bold in (b)).

aromatic (NICS(0) = −5.19 ppm) while the cyclopenta rings are anti-aromatic (NICS(0) = 13.06 ppm). The four N-CH$_2$ protons of butyl chain are deshielded to 5.69 ppm (compared to 4.04 ppm in **4MC-4H**) and are found to have a correlation with 8 'd' (4 × 2 H's) protons appearing at 3.03 ppm. Upon cooling, an apparent high-field shift of the -N−CH$_2$ proton peaks that eventually get overlapped with the solvent peak was observed, most likely due to strong aggregation. In fact, the X-ray crystallographic structure of **4MC-CHO** exhibits a rather small interplanar distance of 3.39 Å, suggesting π−π interactions between two nearby carbazole moieties bearing aldehyde units (Figure S31 in SI). Subsequent correlations of the 'd' with 8 'e' (4 × 2 H's) protons at 2.15 ppm, and 'e' with the 12 'f' (4 × 3 H's) protons at 1.19 ppm were found. That leaves the assignment of mesityl hydrogens to the three sets of signal with 3 integration each, which were found at 5.10, 2.81, and −1.95 ppm, thus assignable to mesityl −CH$_3$ protons. The p-CH$_3$ protons of mesityl groups, being far from macrocyclic ring current, appears at 2.81 ppm, a usual chemical shift for such protons observed for mesityl groups attached to the sp^2 carbon of cyclopenta ring containing a π-extended p-quinodi-methane moiety.[17] The o-CH$_3$ protons appeared separately at 5.10 and −1.95 ppm, which is indicative of the molecule's conformational rigidity in the bowl shape (*vide infra*). The two sets of signals with one integration each from the four mesityl m-H's (total 4 × 2 H's) appeared at 8.23 and 6.64 ppm. Although broad signals were observed due to unavoidable population of triplet species, the NMR spectrum and its overall integration are clearly in agreement with **4MC**.

Although the structure of the precursor **6MC-6H** was confirmed by 2D NOESY NMR spectrum and the structure of the **6MC** was supported by HR MS (Figures S8 and S18 in SI), the variable-temperature ^1H NMR spectra of **6MC** in CD_2Cl_2 are significantly broadened, and no signals could be observed

for protons on the carbazole macrocycle framework even at 183 K (Figure S20 in SI), indicating a larger radical character in comparison to **4MC**. NICS calculations of **6MC** in C_1 symmetry reveal weak aromatic character of the benzenoid rings in the macrocycle NICS(0) ≈ −2.6 ppm), while the cyclopenta rings are less anti-aromatic (NICS(0) = +7.7 ppm) and the N-containing five-membered rings become more aromatic in comparison to **4MC** (Figure 5a). These results
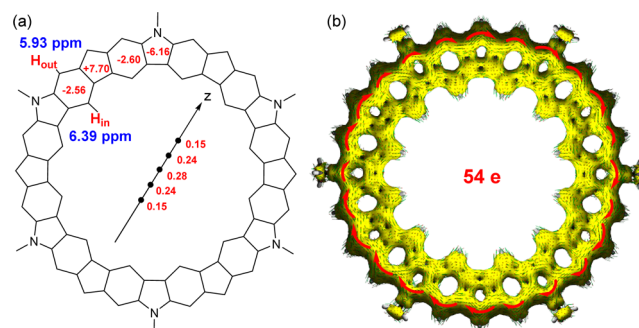

Figure 5. (a) Calculated NICS(0) values and checmial shifts for **6MC** in C_1 symmetry, and an NICS scan along the z axis at the molecular center. (b) Calculated AICD plot of **6MC**; the red arrows indicate clockwise ring current delocalized along the periphery with 54 π electrons.

point toward **6MC** having a larger radical character and, consequently, a higher tendency to populate to paramagnetic species, leading to significant NMR broadening. The chemical shifts for the inner and outer ring protons are calculated to be 6.39 and 5.93 ppm, which however could not be observed due to the existence of significant amount of paramagnetic species even at very low temperature. The z-axis NICS scan at the

center of the macrocycle indicates a nearly non-aromatic character. Accordingly, the AICD plot of **6MC** reveals a disrupted ring current along the periphery (including nitrogen atoms); however, the presence of weak clockwise diatropic ring current with 54 (4n+2, n = 13) π electrons is considered due to the contribution of open-shell poly-radical electronic structure (Figure 5b).

Strong and broad electron spin resonance (ESR) signals with no half-filled transitions were observed (Figure S21 in SI) for both **4MC** and **6MC**, in solid and solution state at room temperature, a typical observation of open-shell singlet systems with large spin-delocalization within the entire molecule. Unfortunately, we are unable to grow single crystals for **4MC** and **6MC** due to the gradual degradation of the samples after various attempts under inert atmosphere, including solvent vapor diffusion, solvent layering, or even under sealed H-tube. Attempts to replace the mesityl substituents by electron-withdrawing pentafluorophenyl and 3,5-bis(trifluoromethyl)-phenyl groups were also conducted; however, the last step oxidative dehydrogenation by DDQ did not work well, making the separation of the target products unsuccessful.

Optical and Electrochemical Properties. DCM solutions of **4MC** and **6MC** exhibit purple and green colors, respectively, and present intriguing deep near-IR (NIR) absorption bands beyond 2000 nm (Figure 6a). For **4MC**, an intense absorption
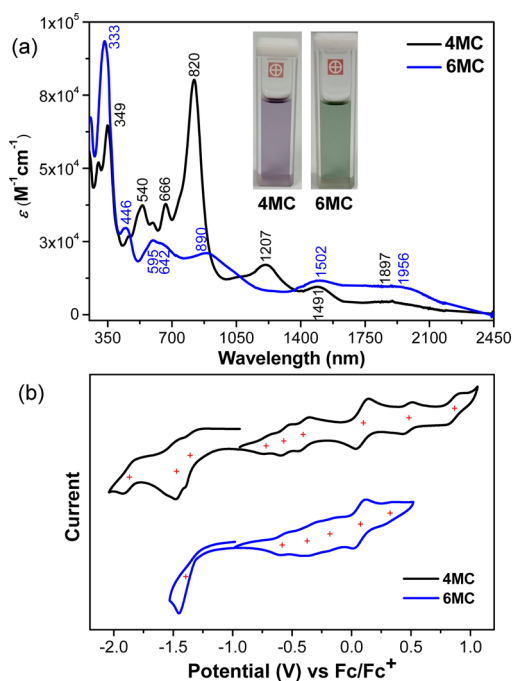

Figure 6. (a) UV–vis–NIR absorption spectra of **4MC** and **6MC** in DCM. Inset are the photos of their solutions. (b) Cyclic voltammo-grams of **4MC** (black) and **6MC** (blue) determined in dry DCM containing 0.1 M n-tetrabutylammonium hexafluorophosphate as electrolyte.

band in the far-red region with maximum at 820 nm is found along with smaller shoulder bands at 666 and 540 nm. A relatively less intense UV–vis band at 349 nm and three NIR bands centered at 1207, 1491, and 1897 nm are also detected. **6MC** shows a similar electronic absorption spectrum to **4MC**, with an intense UV absorption band at 333 nm, a significantly intensity reduced absorption band in the far-red region (890 nm), and two weak absorption bands in the NIR region (1502

and 1956 nm). The optical energy gaps of **4MC** and **6MC**, estimated from the lowest energy absorption onset, are approximately found to be only around 0.52 eV for both molecules, although they have different conjugation sizes. Notably, the higher energy bands at 274–410 nm, which are likely originated from the absorption of aromatic carbazole subunits, are blue-shifted and intensified in **6MC**, indicating a larger radical character.[8c] No significant change in spectral pattern was observed when zinc powder was added to the solutions of **4MC** and **6MC** in DCM, indicating that there are no over-oxidized species (e.g., radical cation) in the purified samples.

Cyclic voltammogram of **4MC** shows six quasi-reversible oxidation waves with half-wave potentials ($E_{1/2}^{ox}$) at −0.71, −0.55, −0.44, 0.08, 0.47, and 0.85 V, and three reduction waves with $E_{1/2}^{red}$ at −1.33, −1.46 and −1.85 V (vs ferrocene/ferrocenium (Fc/Fc$^+$)) (Figure 6b). Compound **6MC** also shows identical multiple anodic oxidations with $E_{1/2}^{ox}$ at −0.57, −0.34, −0.15, 0.07, and 0.32 V, and one irreversible reduction with $E_{1/2}^{red}$ at −1.30 V. The HOMO energy levels of **4MC** and **6MC** are extremely high, at −4.01 and −4.14 eV, respectively, while the LUMO energy levels remain unaffected at −3.51 eV from one to another. The electrochemical energy gaps for **4MC** and **6MC** are estimated to be 0.50 and 0.63 eV, respectively, in consistence with their optical energy gaps.

Ground-State Electronic Structures, Radical Charac-ters, and Excitation Energies. In the following, we perform a detailed theoretical and computational study to investigate the ground-state electronic structure and poly-radical characters of **4MC** and **6MC**. In all calculations presented in this section the mesityl and n-butyl substituents are replaced by hydrogen and methyl substituents, respectively. First, molecular geometries of **4MC** and **6MC** were analyzed using density functional theory (DFT) calculations at the unrestricted B3LYP/6-31G* level.[18] For **4MC**, the energy minimum conformation presents a bowl-like structure with a two-fold alternate conjugated system (C_{2v}), while the completely conjugated structure (C_{4v}) lies at higher energy (6.3 kcal/mol) (Figure 7 and Table 1). The planar
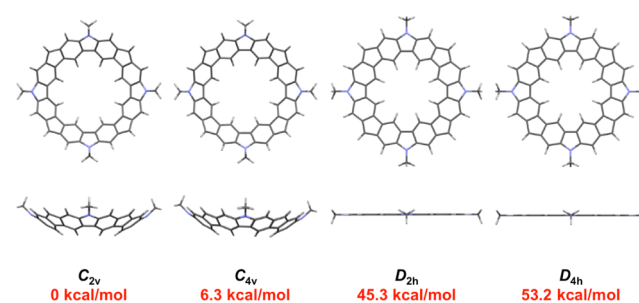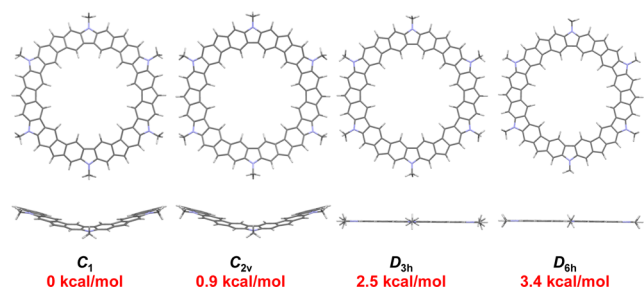

Figure 7. Optimized structures of **4MC** in different symmetry and their relative energies, using UB3LYP/6-31G*.

counterparts of C_{2v} and C_{4v} structures, i.e., D_{2h} and D_{4h}, respectively, are quite strained and appear at much higher energies (>45 kcal/mol). Thus, only C_{2v} and C_{4v} forms are accessible to the ground state of **4MC**.

The energetically lowest geometry of **6MC** presents a non-planar structure with C_1-symmetric three-fold alternate pattern. The C_{2v} symmetric higher conjugated form is found to be rather close in energy (e.g., ΔE = 0.9 kcal/mol) (Figure 8 and Table 1). The planar analogues, with D_{3h} and D_{6h} symmetries, lie at slightly higher energies relative to the C_1 structure (i.e.,

Table 1. Relative Energies, Numbers of Unpaired Electrons, and the Multiple-Radical Characters in Different Symmetries

molecule	point group	energy (kcal/mol)	N_U	y_0	y_1	y_2
4MC	C_{2v}	0	2.14	0.27	0.19	
	C_{4v}	6.3	3.15	1.00	0.27	
	D_{2h}	45.3	2.33	0.33	0.24	
	D_{4h}	53.2	3.21	1.00	0.31	
6MC	C_1	0	3.48	0.31	0.31	0.23
	C_{2v}	0.9	4.14	0.53	0.52	0.27
	D_{3h}	2.5	3.52	0.32	0.32	0.24
	D_{6h}	3.4	4.15	0.53	0.32	0.27

C_1 0 kcal/mol C_{2v} 0.9 kcal/mol D_{3h} 2.5 kcal/mol D_{6h} 3.4 kcal/mol

Figure 8. Optimized structures of **6MC** in different symmetry and their relative energies, using UB3LYP/6-31G*.

2.5 and 3.4 kcal/mol, respectively), which represents a rather small difference, especially compared to the **4MC** case. The larger macrocycle **6MC** mitigates strain, and all four forms contribute considerably to its ground-state geometry. The theoretical predictions for the ground-state geometries of **4MC** and **6MC** molecules are supported by the comparison of the experimental and theoretical infrared spectra (Figure S23 in SI).

In an effort to scrutinize poly-radical character for **4MC** and **6MC**, analysis of the natural orbital (NO) occupations was carried out as computed using restricted active space spin flip method (RAS-SF/6-31G*).[19] The radical character degree of the ground-state singlet was estimated by the number of unpaired electrons (N_U) according to eq 1,[20] where $\{n_i\}$ are the natural occupation numbers from the one-particle density matrix.

$$N_U = \sum_i \left(1 - \mathrm{abs}(1 - n_i)\right) \tag{1}$$

On the basis of occupation numbers of the unoccupied natural orbitals LUNO, LUNO+1, and LUNO+2, the diradical character (y_0), tetraradical (y_1) and hexaradical character (y_2) can be determined, respectively, through the Yamaguchi's indices, y_i, $i = 0, 1, 2$ (eq 2):[21]

$$y_i = 1 - \frac{2T_i}{1 + T_i^2}; \qquad T_i = \frac{n_{\mathrm{HONO}-i} - n_{\mathrm{LUNO}+i}}{2} \tag{2}$$

The radical character indices y_i are well defined for the UHF wave functions, where the $n_{\mathrm{HONO}-i} + n_{\mathrm{LUNO}+i} = 2$ condition applies. Although this is not in general the case for multi determinantal wave functions, the sum condition is virtually satisfied for the RAS-SF ground-state wave functions of **4MC** and **6MC** (Table S5 in SI).

The frontier NO occupancies of **4MC** with C_{2v} and C_{4v} symmetry (Figure 9a), and **6MC** with C_1 and C_{2v} (Figure 9b),
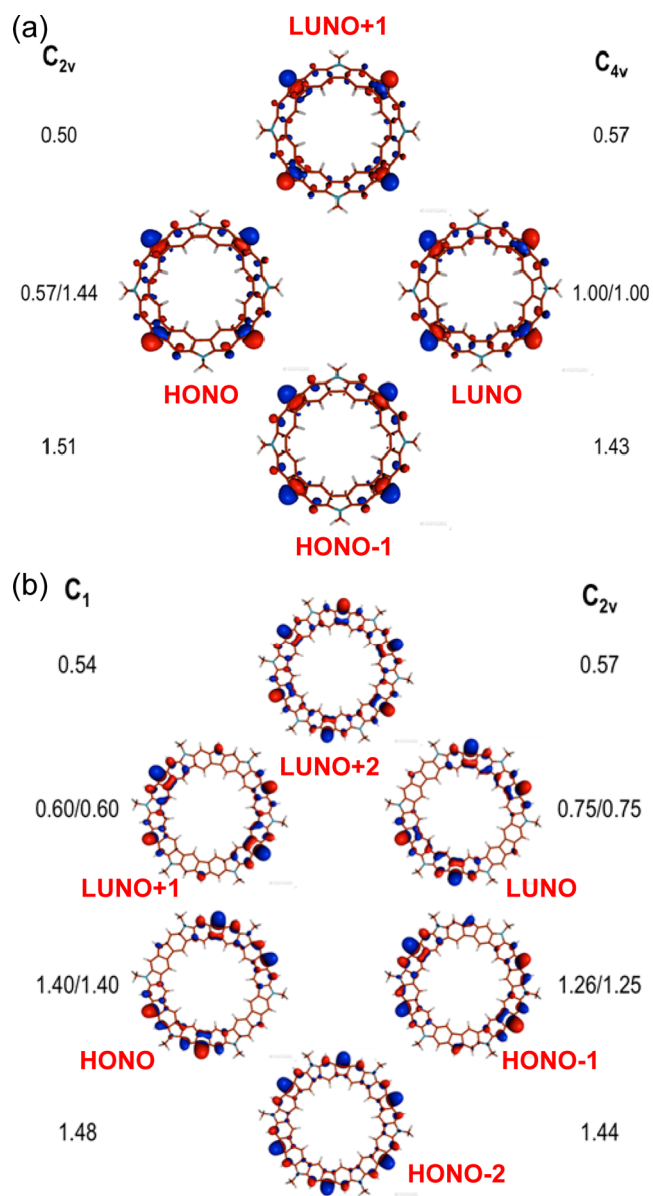
Figure 9. Natural orbital diagrams and occupancy numbers for (a) **4MC** and (b) **6MC** with different symmetry.

clearly show important departures from the non-radical case, i.e., fully occupied and completely empty NOs, suggesting large radical characters for both molecules (Table 1). For example, **4MC** with either symmetry shows large N_U values and moderate tetraradical character ($y_1 = 0.19$ for C_{2v} symmetry and $y_1 = 0.27$ for C_{4v} symmetry) and the higher the symmetry, the larger the radical character, as the C_{4v} structure is correlated to a tetraradical resonance form (Figure 1). **6MC** exhibits a similar trend and all four conformations show moderate diradical, tetraradical and hexaradical characters. Therefore, **4MC** and **6MC** can be regarded as tetraradicaloid and hexaradicaloid, respectively. High odd electron densities are found at the mesityl-linked carbons (Figure 9), which are chemically protected by the bulky groups rendering **4MC** and **6MC** sufficient stability. Calculations also show that both **4MC** and **6MC** have a singlet ground state, and the vertical energy gaps from the ground state to the lowest spin triplet, quintet, and septet states are substantially small (Table 2 and Figure S27 in SI). For example, it is found that the triplet and quintet

Table 2. Calculated (RAS-SF) Vertical Energy Gaps (in kcal/mol) from the Ground-State Singlet to the Lowest Triplet, Quintet, and Septet States of 4MC and 6MC

state	4MC				6MC		
	C_{2v}	C_{4v}	D_{2h}	D_{4h}	C_1	C_{2v}	D_{6h}
triplet	5.5	2.1	4.8	2.0	4.0	1.8	1.8
quintet	13.1	7.6	11.7	7.2	9.3	6.1	5.9
septet					15.5	11.4	11.1

states are 2.1 and 7.6 kcal/mol higher in energy than S$_0$ singlet for **4MC** with C_{4v} symmetry, and for **6MC** with C_{2v} symmetry, the triplet, quintet, and septet states are 1.8, 6.1, and 11.4 kcal/mol higher, respectively. Therefore, by heating, one can expect a transformation to the higher symmetry structures and simultaneously a population of high-spin states that may account for the room-temperature magnetic activity (*vide infra*). On the other hand, broken-symmetry DFT calculations (UB3LYP/6-31G*) had problems to evaluate these open-shell singlet molecules with poly-radical character. In particular, the calculations overestimated the excitation energies (Table S4 in SI).

Vibrational Spectroscopy. Raman and IR spectroscopic measurements of **4MC** and **6MC** give further insight into their ground-state geometries and electronic structures (Figure 10
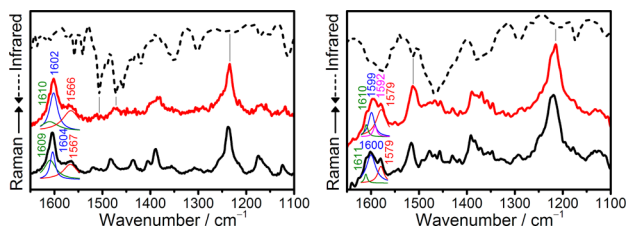

Figure 10. IR spectrum at 400 K (dotted line) and 785 nm Raman spectra (solid line with deconvolutions) in solid state at 80 K (black line) and at 400 K (red line). Left, for **4MC**; right, for **6MC**.

and Figure S24 in SI).[22] The Raman spectrum of **6MC** at 80 K is characterized by three main bands at 1611, 1600, and 1579 cm^{-1}, which are distinctive of exocyclic C=C, CC benzo-aromatic and C=C benzo-quinoidal vibrational stretches, respectively.[8c,d] The presence of these bands indicates that both aromatic and quinoidal carbazole segments are constitutive parts of the ground electronic state. Increase of the temperature to 400 K led to (i) a very slight downshift by 1/1/0 cm^{-1} for the 1611/1600/1579 cm^{-1} bands, which agrees with the small energy interval (Table 1) for the valence automerization and geometric change, and (ii) a new feature at 1592 cm^{-1} appears in the low-frequency side of the 1600 cm^{-1} at 400 K in agreement with the thermal population of triplet species. The Raman spectrum of **4MC** at 80 K is characterized also by three bands at 1609, 1604, and 1567 cm^{-1}, which also exhibit small shifts when increasing the temperature. However, no new bands appear in the spectrum of **4MC** with heating, revealing the larger C_{2v}/C_{4v} energy difference in **4MC** than in **6MC**.

In an attempt to get further insights on the automerization effect, we have compared the Raman and IR spectra of **6MC** at 400 K in the assumption that the mutual exclusion principle should be verified for D_{3h}- and D_{6h}-symmetry point groups. The most IR-active band (at 1466 cm^{-1}) is very weak in Raman and vice versa for the most Raman-active 1513 cm^{-1} band (Figure

10). Nonetheless, for the 1600 cm^{-1} structurally relevant interval, only a partial fulfillment of the IR/Raman complementarity is verified, revealing that a full shift to the D_{3h}/D_{6h} automers is not attained by 80 → 400 K heating. Similarly, in the IR spectrum of **4MC**, bands very strong in IR are weak or very weak in Raman and vice versa, in agreement with the absence of an inversion center in the relevant ground-state molecular symmetry.

Magnetic Properties. The magnetic properties of **4MC** and **6MC**, as powder sample, were further investigated by superconducting quantum interfering device (SQUID) measurements at the 2−380 K temperature interval. **6MC** shows an increasing magnetic susceptibility above 35 K (Figure 11a),
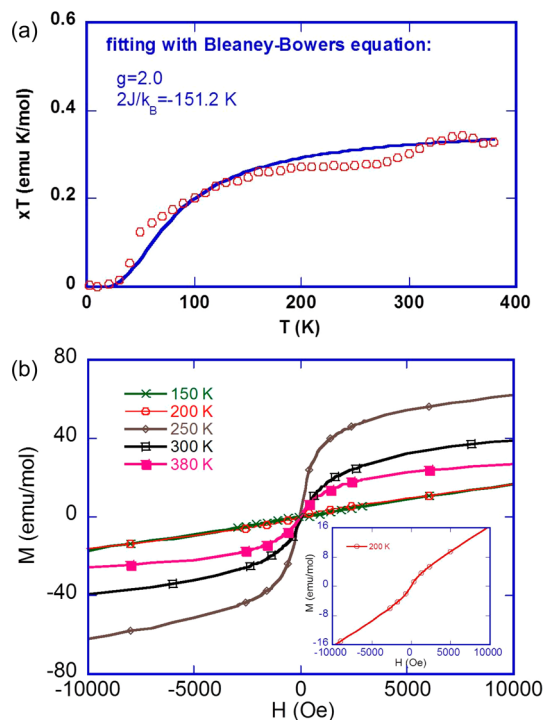

Figure 11. (a) χT−T plot for powder **6MC**. The measured data were plotted as open circles, and the fitting curve was drawn using Bleaney–Bowers equation with g_e = 2.00. (b) Magnetization curves at different temperatures for powder **6MC**.

indicating a singlet ground-state as predicted by calculations and the occupation of paramagnetic state−triplet via thermal excitation. There is another clear increase of magnetic susceptibility around 250 K, which might be associated with excitation into other spin states or a phase transition. As shown in Figure 11b, magnetization curves taken below 200 K are typical for paramagnetism. Interestingly, magnetization measurements for **6MC** clearly shows a weak magnetization starting around 200 K, which reaches a maximum at 250 K and then decreases with increasing temperature until becomes very weak at 380 K (Figure 11b). Such a behavior is similar to long-range ordered ferromagnetic coupling; however, considering the very narrow hysteresis loop, this magnetization is better described as super-paramagnetism. The observed magnetization at room temperature in **6MC** can be rationalized as a consequence of molecular structure rigidity, small energy gap to high-spin states (triplet, quintet, and even septet), and certain unique packing in solid state (not clear at this stage). Due to the complication by the multiple-step thermal transitions combined with the

existence of weak magnetization, the SQUID data were only fitted by Bleaney−Bowers equation[23] based on a singlet−triplet model, with a singlet−triplet energy gap ($\Delta E_{S\text{-}T}$, i.e., $2J/k_B$) of −0.30 kcal/mol. Similar to **6MC**, the SQUID measurements of **4MC** shows an increasing susceptibility above 4 K and relatively weaker magnetization at 300 K (Figure S22 in SI). Fitting of the data by Bleaney−Bowers equation gave a singlet/triplet energy gap of −0.25 kcal/mol. An obvious discrepancy in calculated singlet−triplet energy gap with experimentally observed value still can be seen which may infer that theoretical methods are yet to be verified to fit for estimating singlet−triplet gaps in open-shell systems with poly-radical character.

CONCLUSIONS

In summary, two fully fused quinoidal/aromatic carbazole macrocycles, **4MC** and **6MC**, have been successfully synthesized and isolated. We have demonstrated that both have significant poly-radical characters and very small energy gaps in the ground state. They can be regarded as the first true open-shell organic singlet tetraradicaloid and hexaradicaloid molecules, respectively. Both compounds have small excitation energy gaps and can be thermally populated to high-spin excited states, which results in interesting magnetization behavior even at room temperature. Although the magnetization is very weak, it may imply an alternative approach to design molecular magnets in the future. Assuming that one can synthesize 2D and 3D rigid organic frameworks with poly-radical characters in a singlet ground state, thermal population to high-spin states could become significant, and the long-range ordered alignment of the spin would eventually lead to significant magnetization at higher temperature. Research along this line is underway in our laboratories.

ASSOCIATED CONTENT

Ⓢ Supporting Information

The Supporting Information is available free of charge on the ACS Publications website at DOI: 10.1021/jacs.6b04539.

> Experimental details, NMR and mass spectra, ESR spectra, Raman and IR spectra, and theoretical calculation details (PDF)
> X-ray crystallographic data for **4MC-CHO** (CIF)
> X-ray crystallographic data for **6MC-CHO** (CIF)

AUTHOR INFORMATION

Corresponding Authors
*casado@uma.es
*msedingj@nus.edu.sg
*david.casanova@ehu.eus
*chmwuj@nus.edu.sg

Notes

The authors declare no competing financial interest.

ACKNOWLEDGMENTS

REFERENCES

(1) (a) Sun, Z.; Ye, Q.; Chi, C.; Wu, J. *Chem. Soc. Rev.* **2012**, *41*, 7857. (b) Shimizu, A.; Hirao, Y.; Kubo, T.; Nakano, M.; Botek, E.; Champagne, B. *AIP Conf. Proc.* **2009**, *1504*, 399. (c) Sun, Z.; Zeng, Z.; Wu, J. *Chem. - Asian J.* **2013**, *8*, 2894. (d) Abe, M. *Chem. Rev.* **2013**, *113*, 7011. (e) Sun, Z.; Zeng, Z.; Wu, J. *Acc. Chem. Res.* **2014**, *47*, 2582. (f) Kubo, T. *Chem. Rec.* **2015**, *15*, 218. (g) Zeng, Z.; Shi, X.; Chi, C.; López Navarrete, J. T.; Casado, J.; Wu, J. *Chem. Soc. Rev.* **2015**, *44*, 6578. (h) Kubo, T. *Chem. Lett.* **2015**, *44*, 111. (i) Nakano, M. *Excitation Energies and Properties of Open-Shell Singlet Molecules*; Springer: New York, 2014.

(2) Kamada, K.; Ohta, K.; Kubo, T.; Shimizu, A.; Morita, Y.; Nakasuji, K.; Kishi, R.; Ohta, S.; Furukawa, S. I.; Takahashi, H.; Nakano, M. *Angew. Chem., Int. Ed.* **2007**, *46*, 3544.

(3) Koike, H.; Chikamatsu, M.; Azumi, R.; Tsutsumi, J.; Ogawa, K.; Yamane, W.; Nishiuchi, T.; Kubo, T.; Hasegawa, T.; Kanai, K. *Adv. Funct. Mater.* **2016**, *26*, 277.

(4) Son, Y. W.; Cohen, M. L.; Louie, S. G. *Phys. Rev. Lett.* **2006**, *97*, 216803.

(5) See examples of quinoidal thiophene- and thienoacene-based diradicaloids: (a) Takahashi, T.; Matsuoka, K. I.; Takimiya, K.; Otsubo, T.; Aso, Y. *J. Am. Chem. Soc.* **2005**, *127*, 8928. (b) Ortiz, R. P.; Casado, J.; Hernandez, V.; López Navarrete, J. T.; Viruela, P. M.; Orti, E.; Takimiya, K.; Otsubo, T. *Angew. Chem., Int. Ed.* **2007**, *46*, 9057. (c) Canesi, E. V.; Fazzi, D.; Colella, L.; Bertarelli, C.; Castiglioni, C. *J. Am. Chem. Soc.* **2012**, *134*, 19070. (d) Rudebusch, G. E.; Fix, A. G.; Henthorn, H. A.; Vonnegut, C. L.; Zakharov, L. N.; Haley, M. M. *Chem. Sci.* **2014**, *5*, 3627. (e) Shi, X.; Burrezo, P. M.; Lee, S.; Zhang, W.; Zheng, B.; Dai, G.; Chang, J.; López Navarrete, J. T.; Huang, K.-W.; Kim, D.; Casado, J.; Chi, C. *Chem. Sci.* **2014**, *5*, 4490. (f) Streifel, B. C.; Zafra, J. L.; Espejo, G. L.; Gómez-García, C. J.; Casado, J.; Tovar, J. D. *Angew. Chem., Int. Ed.* **2015**, *54*, 5888. (g) Shi, X.; Quintero, E.; Lee, S.; Jing, L.; Herng, T. S.; Zheng, B.; Huang, K.-W.; López Navarrete, J. T.; Ding, J.; Kim, D.; Casado, J.; Chi, C. *Chem. Sci.* **2016**, *7*, 3036.

(6) See examples of bisphenalenyl-based diradicaloids: (a) Ohashi, K.; Kubo, T.; Masui, T.; Yamamoto, K.; Nakasuji, K.; Takui, T.; Kai, Y.; Murata, I. *J. Am. Chem. Soc.* **1998**, *120*, 2018. (b) Kubo, T.; Sakamoto, M.; Akabane, M.; Fujiwara, Y.; Yamamoto, K.; Akita, M.; Inoue, K.; Takui, T.; Nakasuji, K. *Angew. Chem., Int. Ed.* **2004**, *43*, 6474. (c) Kubo, T.; Shimizu, A.; Sakamoto, M.; Uruichi, M.; Yakushi, K.; Nakano, M.; Shiomi, D.; Sato, K.; Takui, T.; Morita, Y.; Nakasuji, K. *Angew. Chem., Int. Ed.* **2005**, *44*, 6564. (d) Shimizu, A.; Uruichi, M.; Yakushi, K.; Matsuzaki, H.; Okamoto, H.; Nakano, M.; Hirao, Y.; Matsumoto, K.; Kurata, H.; Kubo, T. *Angew. Chem., Int. Ed.* **2009**, *48*, 5482. (e) Shimizu, A.; Kubo, T.; Uruichi, M.; Yakushi, K.; Nakano, M.; Shiomi, D.; Sato, K.; Takui, T.; Hirao, Y.; Matsumoto, K.; Kurata, H.; Morita, Y.; Nakasuji, K. *J. Am. Chem. Soc.* **2010**, *132*, 14421. (f) Shimizu, A.; Hirao, Y.; Matsumoto, K.; Kurata, H.; Kubo, T.; Uruichi, M.; Yakushi, K. *Chem. Commun.* **2012**, *48*, 5629.

(7) See examples of zethrene-based diradicaloids: (a) Sun, Z.; Huang, K.-W.; Wu, J. *J. Am. Chem. Soc.* **2011**, *133*, 11896. (b) Li, Y.; Heng, K.-W.; Lee, B. S.; Aratani, N.; Zafra, J. L.; Bao, N.; Lee, R.; Sung, Y. M.; Sun, Z.; Huang, K.-W.; Webster, R. D.; López Navarrete, J. T.; Kim, D.; Osuka, A.; Casado, J.; Ding, J.; Wu, J. *J. Am. Chem. Soc.* **2012**, *134*, 14913. (c) Sun, Z.; Lee, S.; Park, K.; Zhu, X.; Zhang, W.; Zheng, B.; Hu, P.; Zeng, Z.; Das, S.; Li, Y.; Chi, C.; Li, R.; Huang, K.; Ding, J.; Kim, D.; Wu, J. *J. Am. Chem. Soc.* **2013**, *135*, 18229. (d) Das, S.; Lee, S.; Son, M.; Zhu, X.; Zhang, W.; Zheng, B.; Hu, P.; Zeng, Z.; Sun, Z.; Zeng, W.; Li, R.-W.; Huang, K.-W.; Ding, J.; Kim, D.; Wu, J. *Chem. - Eur. J.* **2014**, *20*, 11410. (e) Ni, Y.; Lee, S.; Son, M.; Aratani, N.; Ishida, M.; Yamada, H.; Chang, Y.-T.; Furuta, H.; Kim, D.; Wu, J. *Angew. Chem., Int. Ed.* **2016**, *55*, 2815. (f) Hu, P.; Lee, S.; Park, K. H.; Das, S.; Herng, T. S.; Gonçalves, T. P.; Huang, K.-W.; Ding, J.; Kim, D.; Wu, J. *J. Org. Chem.* **2016**, *81*, 2911. (g) Zeng, W. D.; Sun, Z.; Herng, T. S.; Gonçalves, T. P.; Gopalakrishna, T. Y.; Huang, K.-W.; Ding, J.; Wu, J.

Angew. Chem., Int. Ed. **2016**, DOI: 10.1002/anie.201602997. (h) Yadav, P.; Das, S.; Phan, H.; Herng, T. S.; Ding, J.; Wu, J. *Org. Lett.* **2016**, DOI: 10.1021/acs.orglett.6b01196.

(8) See examples of extended *p*-quinodimethane-based diradicaloids: (a) Zhu, X.; Tsuji, H.; Nakabayashi, H.; Ohkoshi, S.; Nakamura, E. *J. Am. Chem. Soc.* **2011**, *133*, 16342. (b) Zeng, Z.; Sung, Y. M.; Bao, N.; Tan, D.; Lee, R.; Zafra, J. L.; Lee, B. S.; Ishida, M.; Ding, J.; López Navarrete, J. T.; Li, Y.; Zeng, W.; Kim, D.; Huang, K.-W.; Webster, R. D.; Casado, J.; Wu, J. *J. Am. Chem. Soc.* **2012**, *134*, 14513. (c) Zeng, Z.; Ishida, M.; Zafra, J. L.; Zhu, X.; Sung, Y. M.; Bao, N.; Webster, R. D.; Lee, B. S.; Li, R.-W.; Zeng, W.; Li, Y.; Chi, C.; Navarrete, J. T. L.; Ding, J.; Casado, J.; Kim, D.; Wu, J. *J. Am. Chem. Soc.* **2013**, *135*, 6363. (d) Zeng, Z.; Lee, S.; Zafra, J. L.; Ishida, M.; Zhu, X.; Sun, Z.; Ni, Y.; Webster, R. D.; Li, R.-W.; López Navarrete, J. T.; Chi, C.; Ding, J.; Casado, J.; Kim, D.; Wu, J. *Angew. Chem., Int. Ed.* **2013**, *52*, 8561. (e) Zeng, Z.; Lee, S.; Zafra, J. L.; Ishida, M.; Bao, N.; Webster, R. D.; López Navarrete, J. T.; Ding, J.; Casado, J.; Kim, D.-H.; Wu, J. *Chem. Sci.* **2014**, *5*, 3072. (f) Zeng, Z.; Lee, S.; Son, M.; Fukuda, K.; Burrezo, P. M.; Zhu, X.; Qi, Q.; Li, R.-W.; Navarrete, J. T. L.; Ding, J.; Casado, J.; Nakano, M.; Kim, D.; Wu, J. *J. Am. Chem. Soc.* **2015**, *137*, 8572. (g) Lim, Z. L.; Zheng, B.; Huang, K.-W.; Liu, Y.; Wu, J. *Chem. - Eur. J.* **2015**, *21*, 18724.

(9) See examples of anthene-based diradicaloids: (a) Konishi, A.; Hirao, Y.; Nakano, M.; Shimizu, A.; Botek, E.; Champagne, B.; Shiomi, D.; Sato, K.; Takui, T.; Matsumoto, K.; Kurata, H.; Kubo, T. *J. Am. Chem. Soc.* **2010**, *132*, 11021. (b) Konishi, A.; Hirao, Y.; Matsumoto, K.; Kurata, H.; Kishi, R.; Shigeta, Y.; Nakano, M.; Tokunaga, K.; Kamada, K.; Kubo, T. *J. Am. Chem. Soc.* **2013**, *135*, 1430. (c) Liu, J.; Ravat, P.; Wagner, M.; Baumgarten, M.; Feng, X.; Müllen, K. *Angew. Chem., Int. Ed.* **2015**, *54*, 12442.

(10) See examples of indenofluorene-based diradicaloids: (a) Chase, D. T.; Rose, B. D.; McClintock, S. P.; Zakharov, L. N.; Haley, M. M. *Angew. Chem., Int. Ed.* **2011**, *50*, 1127. (b) Shimizu, A.; Tobe, Y. *Angew. Chem., Int. Ed.* **2011**, *50*, 6906. (c) Shimizu, A.; Kishi, R.; Nakano, M.; Shiomi, D.; Sato, K.; Takui, T.; Hisaki, I.; Miyata, M.; Tobe, Y. *Angew. Chem., Int. Ed.* **2013**, *52*, 6076. (d) Miyoshi, H.; Nobusue, S.; Shimizu, A.; Hisaki, I.; Miyata, M.; Tobe, Y. *Chem. Sci.* **2014**, *5*, 163. (e) Shimizu, A.; Nobusue, S.; Miyoshi, H.; Tobe, Y. *Pure Appl. Chem.* **2014**, *86*, 517. (f) Luo, D.; Lee, S.; Zheng, B.; Sun, Z.; Zeng, W.; Huang, K.-W.; Furukawa, K.; Kim, D.; Webster, R. D.; Wu, J. *Chem. Sci.* **2014**, *5*, 4944.

(11) (a) Fujita, M.; Wakabayashi, K.; Kusakabe, K. *J. Phys. Soc. Jpn.* **1996**, *65*, 1920. (b) Nakada, K.; Fujita, M.; Dresselhaus, G.; Dresselhaus, M. S. *Phys. Rev. B: Condens. Matter Mater. Phys.* **1996**, *54*, 17954. (c) Bendikov, M.; Duong, H. M.; Starkey, K.; Houk, K. N.; Carter, E. A.; Wudl, F. *J. Am. Chem. Soc.* **2004**, *126*, 7416. (d) Jiang, D.; Dai, S. *J. Phys. Chem. A* **2008**, *112*, 332. (e) Mizukami, W.; Kurashige, Y.; Yanai, T. *J. Chem. Theory Comput.* **2013**, *9*, 401. (f) Das, A.; Muller, T.; Plasser, F.; Lischka, H. *J. Phys. Chem. A* **2016**, *120*, 1625.

(12) Nobusue, S.; Miyoshi, H.; Shimizu, A.; Hisaki, I.; Fukuda, K.; Nakano, M.; Tobe, Y. *Angew. Chem., Int. Ed.* **2015**, *54*, 2090.

(13) Hu, P.; Lee, S.; Herng, S. T.; Aratani, N.; Goncalves, T. P.; Qi, Q.; Shi, X.; Yamada, H.; Huang, K. − W.; Ding, J.; Kim, D.; Wu, J. *J. Am. Chem. Soc.* **2016**, *138*, 1065.

(14) (a) Montgomery, L. K.; Huffman, J. C.; Jurczak, E. A.; Grendze, M. P. *J. Am. Chem. Soc.* **1986**, *108*, 6004. (b) Beaudoin, D.; Levasseur-Grenon, O.; Maris, T.; Wuest, J. D. *Angew. Chem., Int. Ed.* **2016**, *55*, 894.

(15) Myśliwiec, D.; Stępień, M. *Angew. Chem., Int. Ed.* **2013**, *52*, 1713.

(16) Li, Z.; Liu, Y.; Yu, G.; Wen, Y.; Guo, Y.; Ji, L.; Qin, J.; Li, Z. *Adv. Funct. Mater.* **2009**, *19*, 2677.

(17) Rose, D. B.; Vonnegut, C. L.; Zakharov, L. N.; Haley, M. M. *Org. Lett.* **2012**, *14*, 2426.

(18) Discussion on the validity of UB3LYP geometries, open-shell singlet nature of the ground state of **4MC** and **6MC** molecules, and comparison to LC-UBLYP and SF-BHHLYP results can be found in the Supporting Information.

(19) Casanova, D.; Head-Gordon, M. *Phys. Chem. Chem. Phys.* **2009**, *11*, 9779.

(20) Head-Gordon, M. *Chem. Phys. Lett.* **2003**, *372*, 508.

(21) Minami, T.; Nakano, M. *J. Phys. Chem. Lett.* **2012**, *3*, 145.

(22) Casado, J.; Ortiz, R. P.; López Navarrete, J. T. *Chem. Soc. Rev.* **2012**, *41*, 5672.

(23) Bleaney, B.; Bowers, K. D. *Proc. R. Soc. London, Ser. A* **1952**, *214*, 451.